ACS APPLIED NANO MATERIALS

www.acsanm.org Article

Super-Stable High-Quality Few-Layer Black Phosphorus for Photonic Applications

Dongying Li, Yueyang Yu, and Cun-Zheng Ning*

Cite This: *ACS Appl. Nano Mater.* 2021, 4, 4746−4753 Read Online

ACCESS | Metrics & More | Article Recommendations | Supporting Information

ABSTRACT: Few-layer black phosphorus (BP) is one of the most important 2D materials due to its strongly layer-dependent quantized band structure, which leads to wavelength tunable emission and absorption properties. Such properties are essential for a variety of photonic device applications such as lasers, detectors, and modulators in a wide range of near-infrared wavelengths. However, the material quality and stability have become a bottleneck along with other challenges such as poor light emission properties and considerable uncertainty of basic material parameters. In this paper, we developed a systematic strategy for preparing high-quality stable few-layer BP samples by combining O_2 plasma etching, boron nitride sandwiching, and subsequent thermal annealing. Our strategy has successfully produced few-layer BP samples with a record-long lifetime, with 80% of photoluminescence intensity remaining after 7 months. Importantly, we found that lattice reconstruction and reparation of oxidized BP surfaces increased BP thickness by one monolayer, leading to the restoration of BP crystal structure, improved material quality and stability, and restoration of intrinsic optical properties. As a result, 200× PL enhancement and 2× line width reduction are achieved, allowing the establishment of a more definite relationship between the layer number and PL energies for the first time. Our results could help unleash the full potential of few-layer BP in photonics applications in a wide range of near-infrared wavelengths.

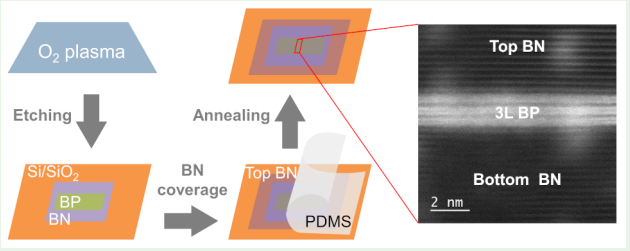

KEYWORDS: *few-layer black phosphorus, photoluminescence, stability, annealing, lattice reconstruction*

INTRODUCTION

Few-layer black phosphorus (FLBP) has been studied extensively since its rediscovery[1−3] due to its remarkable electronic and optical properties: higher carrier mobility than transition metal dichalcogenides (TMDCs), a direct bandgap tunable through the thickness or layer number, and its unique in-plane anisotropy. By varying the thickness of BP from 46 nm (bulk)[4] to 0.5 nm (monolayer),[5] the photoluminescence (PL) peak energy changes from ∼0.33 to ∼1.75 eV, corresponding to a vast and significant mid- to near-infrared (IR) wavelength range from 3.7 to 0.71 μm. In the mid-IR range, a BP-based light-emitting diode (LED)[6,7] has been demonstrated to show comparable external quantum efficiency to that of traditional II−VI and III−V LEDs. For the near-IR range (0.8−2.5 μm), BP is one of the very few 2D layered materials that emit in the telecom wavelength bands (1260−1625 nm).[8] This makes few-layer BP one of the very few most promising candidates as light emission devices of atomic-layer thickness integrable on a Si substrate, especially compared to $MoTe_2$[9,10] due to much smaller Si absorption at longer wavelengths. However, the thickness-sensitive reactivity of BP and O_2 makes FLBP much more unstable than thick BP[11] and the severe instability of FLBP hinders its application in near-IR photonics. Therefore, the preparation of stable and high-quality FLBP is essential to benefit from the superior optical and electronic properties of FLBP.

Although the wavelength-tunable optical emission of FLBP through the change of layer number has been demonstrated by PL measurements,[4,8,12,13] there still exist substantial discrepancies in the relationship between PL peak wavelengths and layer numbers. For instance, the reported emission wavelengths of three-layer (3L) BP vary from 1268 nm[8] to 1470 nm[14] (room temperature) to 1570 nm (77 K).[12] Similar inconsistency exists for other layer numbers, representing a fundamentally unsatisfactory situation of the current understanding of FLBP material. The root cause for this situation lies in uneven sample quality and severe instability of FLBP. Due to the high reactivity of freshly exfoliated FLBP with O_2 and H_2O in the ambient environment, PL of FLBP experiences fast degradation[13,15] followed by spectra blueshift within minutes under laser excitation.[16] In addition, the PL spectrum of BP is often very broad and weak, containing emissions from intrinsic

Received: February 3, 2021
Accepted: April 8, 2021
Published: April 20, 2021

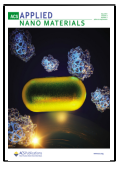

https://doi.org/10.1021/acsanm.1c00351
ACS Appl. Nano Mater. 2021, 4, 4746−4753

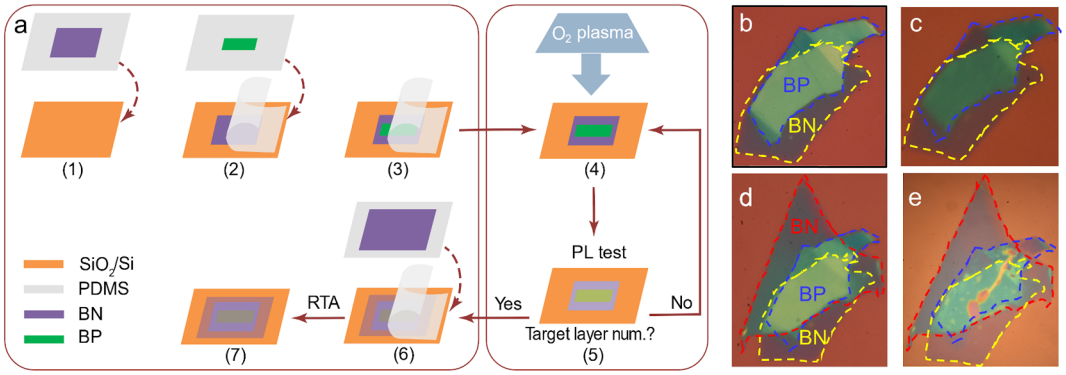

Figure 1. (a) Schematic of the procedure to fabricate BN/BP/BN structure: (1) transfer a layer of BN (10−20 nm, exfoliated from a bulk BN) as the bottom BN onto a SiO_2/Si substrate, (2) transfer thick BP (~10 nm, exfoliated from a bulk) onto BN, (3) BP/BN before plasma etching, (4) O_2 plasma etching of BP/BN, (5) PL test to check if desired wavelength/layer thickness is obtained, (6) transfer the top BN (10−20 nm) onto etched BP/BN, (7) rapidly anneal the obtained BN/BP/BN structure at 450 °C. (b−e) Optical images of the fabricated sample. (b) Before O_2 plasma etching [(3) in (a)]. (c) After 4 min etching [(5) in (a)]. (d) After top BN coverage [(6) in (a)]. (e) After 5 min annealing at 450 °C [(7) in (a)].

excitonic species and many other defects and impurities, often attributed to different oxide species.[16,17] The sample instability or degradation exacerbates the situation.[18−20] Such distortion of intrinsic emission spectrum by defects-related emissions likely contributes to the uncertainty of the layer-number dependence of emission peaks.

These issues mentioned above highlight the fundamental importance of sample quality of FLBP in understanding the unique physics of FLBP and in exploring device applications. Therefore, the preparation of stable high-quality FLBP samples and restoration of their intrinsic emission properties are the key to resolving the current issues and challenges. Even though various preparation methods of FLBP have been developed, the stability of PL properties (such as intensity, line width, and peak position) of FLBP samples remains poor and are not often systematically studied. Exfoliation (mechanical[5,8] and liquid-phase[21−23]) and etching (thermal annealing,[24,25] UV light,[26] plasma[13,27,28]) are the two most common methods of sample preparation for FLBP. Etching techniques such as plasma etching start from thicker BP, which can be exfoliated in the ambient environment and can produce FLBP samples more efficiently. But the sample quality, especially the emission properties of FLBP obtained from etching, varies significantly due to the difficulty of controlling etching conditions. A special feature of etched FLBP is the formation of a top highly oxidized layer after etching,[13,25,26] which is always defective and amorphous. To be consistent with the previous literature, we refer to such a layer as the P_xO_y layer in this paper. Even though the P_xO_y layer can slow down the degradation rate of inner BP layers as demonstrated,[13,25,26] the associated defective interface can undermine the intrinsic properties of inner BP layers as evidenced by weak and broad PL spectra after O_2 plasma etching in our following discussions.

Among various exfoliation methods, there exists a trade-off between material quality and yield. Mechanical exfoliation is supposed to provide the most intrinsic 2D material. However, FLBP is strongly reactive in the ambient environment, and the thinner it is, the more reactive it is.[18] Therefore, a controllable environment such as an inert gas-filled glovebox[12] is required to exfoliate FLBP with high quality. Such environment constraints may lower the yield of sample preparation due to operation difficulty. To prevent environmental reaction and associated degradation of FLBP, protection of FLBP is essential to achieve high-quality samples. Protection methods include organic coating,[29,30] chemical functionalization,[31,32] atomic layer deposition (ALD) capping,[13,33,34] and coverage by 2D flakes.[35−37] Discussions are rather limited on various protection techniques in terms of quality and stability of optical properties. PMMA-coated BP (<10 nm) still experiences severe degradation as reflected by attenuation of Raman signals after 13 days in air.[29] BP flakes (~10 nm) passivated by covalent functionalization showed changes of electronic properties due to introduced bonds between BP and passivation chemicals, despite the almost intact morphology after 25 days in air.[31] Up to now, ALD Al_2O_3 capping of O_2 plasma etched 2LBP shows the best protection capability, with PL still observable after 2 months in air.[13] However, the influences of the extra ALD step in the prepared FLBP are unclear. Passivation of BP by boron nitride (BN) was also reported,[12,36] but its effects on optical emission were not studied, especially on the stability of PL intensity.

Realizing the fundamental importance of the sample quality in the study of FLBP and the lack of a method to prepare high-quality FLBP with long-term stability, we have attempted in this paper to develop a systematic strategy to prepare stable, high-quality FLBP samples with the explicit intention of improving or restoring intrinsic optical properties. Our new strategy combines three critical steps in succession: (1) O_2 plasma etching of thick BP layers exfoliated from bulk; (2) BN encapsulation from both sides to protect FLBP; and (3) rapid thermal annealing (RTA) at 450 °C, which is above FLBP's decomposition temperature. We show that the high-temperature annealing under BN protection can repair the defective and amorphous P_xO_y layer caused by etching. Our comprehensive study on the FLBP samples before and after annealing demonstrates our samples' overall superiority. Dramatically improved material properties include record-long stability of PL over 7 months, reduced PL line width by a factor of 2, improved anisotropy by as much as a factor of 1.7, and 2 orders of magnitude enhancement of PL intensity after the RTA process. Moreover, we have significantly narrowed the uncertainty ranges of PL peak energies of FLBPs by 7 times, allowing a more precise relationship between layer number and PL peak energies.

https://doi.org/10.1021/acsanm.1c00351
ACS Appl. Nano Mater. 2021, 4, 4746−4753

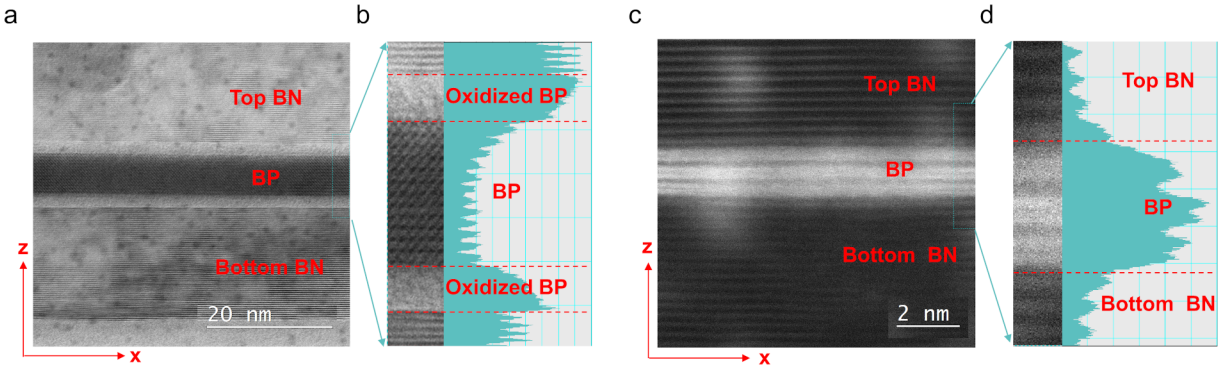

Figure 2. Cross-sectional STEM images for unetched (exfoliated) BP after annealing at 225 °C (a, b) and for etched BP after annealing at 450 °C (c, d) both protected by BN layers. (a) Annular dark-field (ADF) image for the exfoliated (without etching) BP encapsulated by BN. (b) Zoom-in of the segment of (a) in dashed rectangle and its corresponding intensity profile along the *z*-direction, where amorphous oxidized layers can be seen at the two interfaces. (c) ADF image of a layer of etched BP encapsulated by BN from both sides. (d) Zoom-in of the segment of (c) in dashed rectangle and its corresponding intensity profile along the *z*-direction, where three BP layers are clearly visible without amorphous oxidized layers at the two interfaces.

RESULTS AND DISCUSSION

Sample Preparation. The schematic procedure of our method of FLBP preparation is shown in Figure 1a. First, BN flakes of 10−20 nm in thickness are exfoliated onto PDMS and transferred to a SiO_2/Si substrate from PDMS. This step can improve the yield of BN exfoliation and the location controllability of BN flakes. Next, the same method is used to exfoliate and transfer a BP layer of ∼10 nm in thickness onto BN placed on SiO_2/Si in the first step. Then BP/BN structure is etched by O_2 plasma (see Methods for details) to thin down BP and followed by PL measurement to determine the layer number through PL peak wavelengths. If the PL peak wavelength is longer than desired (or the BP thickness is thicker than desired), further etching will be carried out until the desired wavelength is reached. After etching, a second BN layer with a similar thickness as the bottom BN is transferred as a top protective cover of the BP sample. Finally, the BN/BP/BN is annealed at 450 °C in Ar atmosphere for 5 min to achieve better contact between BN and BP and repair the top defective and amorphous P_xO_y layer. Temperature-dependent thermal processing of BP is an interesting issue of study. Through optical imaging and in situ scanning/transmission electron microscopy study, the decomposition temperature of FLBP is determined between 300 and 400 °C.[38,39] With BN encapsulation from both sides, BP can stand up to 500 °C annealing temperature and high-temperature annealing can significantly reduce charge traps.[36] Our experiment showed almost no change of PL's optical properties upon RTA up to 375 °C (see Supporting Information S1). When the RTA temperature was increased to 450 °C, PL was much improved after annealing, as we will discuss later on.

Interface Lattice Reconstruction through High-Temperature Annealing. Cross-sectional scanning transmission electron microscopy (STEM) study was performed to study the interfaces of BN/BP/BN samples and possible effects of thermal annealing. Figure 2a,b shows the STEM images of a BN/BP/BN structure where the middle BP layer was exfoliated from bulk BP. This sample without plasma etching is supposed to be less defective than the etched sample. The sample was annealed at 225 °C for 1.5 min in Ar atmosphere to improve the interface contacts between BP and BN while minimizing the potential adverse effects on the integrity of BP. As shown in Figure 2a,b, amorphous layers exist at interfaces on both sides of the BP due to rapid oxidation after exfoliation. Similar amorphous layers were reported before and were supposed to be oxidized BP.[24,40] To see the effects of RTA at a higher temperature, above the decomposition temperature of BP, we performed RTA on another BN/BP/BN sample at 450 °C for 5 min, and the corresponding STEM images are shown in Figure 2c,d, where the middle BP layers were produced through O_2 plasma etching as described in Figure 1. Three BP layers can be clearly recognized, and no top amorphous oxide layer exists at either interface. This is an interesting and important phenomenon. Given the existence of an amorphous P_xO_y layer on the top surface of BP right after O_2 plasma etching[13] or before RTA, the lack of an amorphous layer in the STEM image shows a clear sign of reconstruction of the interface lattice in BN/P_xO_y-BP/BN under RTA at a relatively high temperature. The consequence of such interface reconstruction and BP quality restoration on optical properties will be discussed further to support such a conclusion. By comparing structures in Figure 2a,c, it seems that 225 °C is not high enough to enable P_xO_y decomposition and surface reconstruction of oxidized BP.

Comparison of PL Properties. An extensive PL study was carried out throughout this paper at various stages, and details are described in Methods. Figure 3 shows a comparison of PL characteristics for the etched BP samples before and after annealing at the same spots. The normalized PL comparison in Figure 3a represents general changes in PL spectrum through RTA: (1) clear redshift of PL peak wavelengths; (2) line width narrowing. It is interesting to notice that the amount of redshift is roughly equivalent to increasing the layer thickness by one monolayer after annealing for all three samples with different thicknesses. Note that there is also PL contribution from the 3L thick BP for the 5L BP after the annealing (see the top panel of Figure 3a). Such inhomogeneity of sample thickness derives mainly from the nonuniform thickness of the original exfoliated thick BP and survived the etching and annealing processes. However, the main feature of the annealing remains that the redshift of the PL peak corresponds to a one-layer increase in thickness (see Figure 3a; Figure S4 in Supporting Information section S4). The redshift in PL is consistent with the interface reconstruction of BN/P_xO_y-BP/BN mentioned above, as is explained in the following. Before annealing, the top surface of the sample was covered by a

https://doi.org/10.1021/acsanm.1c00351
ACS Appl. Nano Mater. 2021, 4, 4746−4753

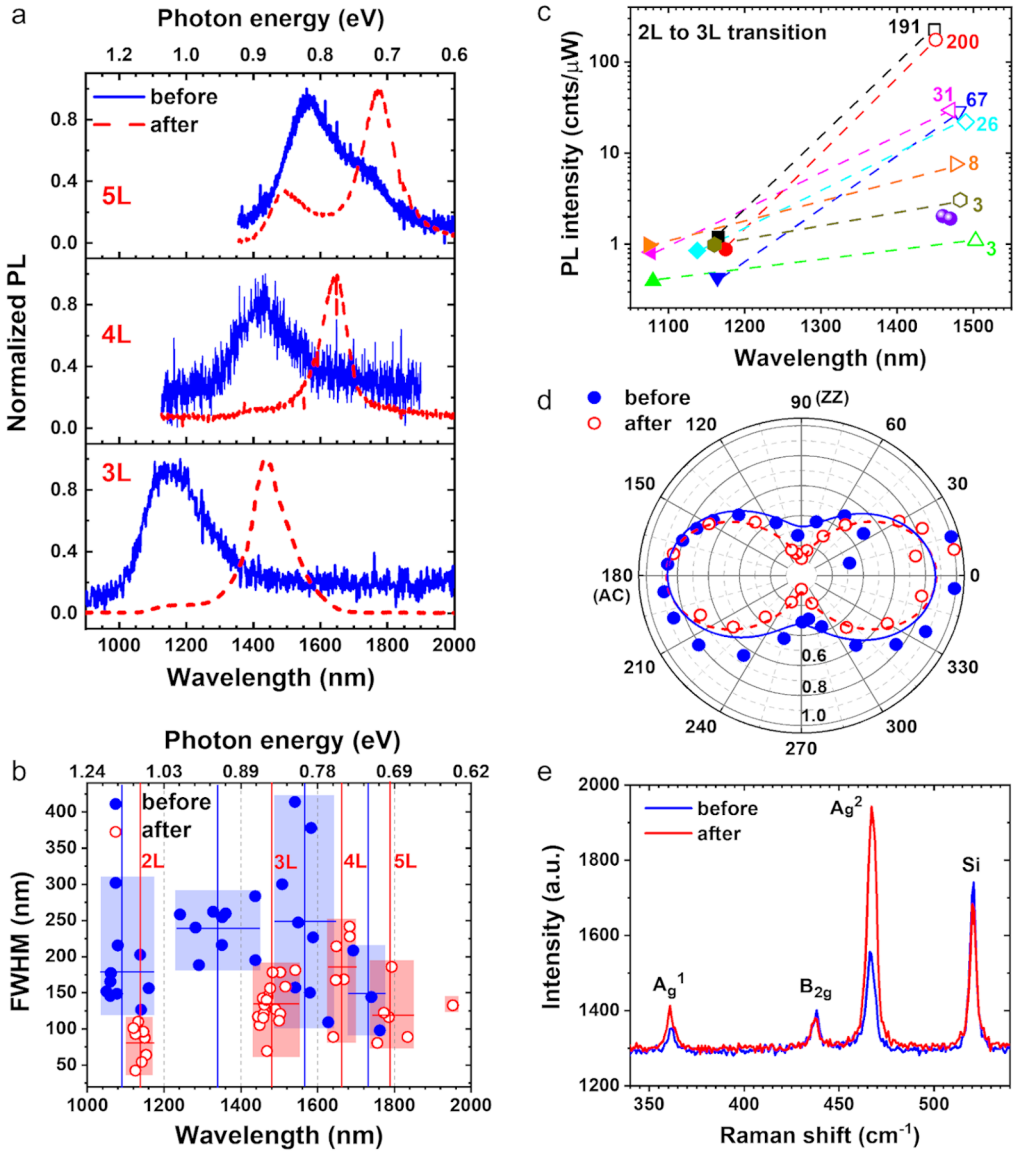

Figure 3. (a) Comparison of the normalized PL spectra before and after annealing for 3L, 4L, and 5L BP. Note that the layer numbers refer to those of samples after annealing. (b) PL line width (fwhm) vs peak wavelength before (blue dots) and after (red circles) annealing. In total, 30 and 37 points on 17 samples were measured before and after annealing, respectively. Blue and red rectangle bands indicate the spreads of peak wavelengths and line widths for different layer numbers. Blue and red solid lines represent the average values of wavelength and fwhm for all dots in each rectangle. The averaged wavelengths after annealing (vertical red lines) are 1137, 1479, 1662, and 1788 nm. (c) Comparison of PL intensity vs peak wavelength before (filled symbols) and after (unfilled symbols) annealing for 7 samples (measured at 8 spots). Numbers next to each unfilled symbol represent the factor of PL enhancement of each sample. The two violet spheres represent PL intensities and wavelengths of typical exfoliated 3L BP (see Supporting Information S2). (d) PL intensity as the excitation polarization rotates through 360° before (blue dots) and after (red circles) annealing. (e) Typical Raman spectra comparison of FLBP before and after annealing.

highly defective and amorphous P_xO_y layer caused by the plasma etching. The corresponding PL spectra are weak and broad. In addition to the redshift of the PL peak, the annealing leads to the disappearance of the amorphous layer (as shown in Figure 2c,d), indicating the reconstruction of the P_xO_y−BP interface. Interestingly, the amount of redshift for all layer numbers we studied is equivalent to the increase of the layer number by one. In other words, the annealing at 450 °C converted the initial defective P_xO_y−N-layer BP into $(N + 1)$-layer BP with the largely restored crystal structure and optical quality. Figure 3b shows a summary of PL measurements with the PL peak wavelengths and line widths (fwhm) extracted from spectra like Figure 3a for all 17 prepared samples of different thickness by the method in Figure 1a before and after annealing. The blue (red) rectangles represent the range of PL parameters (wavelength and line width) before (after) annealing. The spread (or uncertainty) of PL-peak wavelengths for a given BP thickness is in the 150−200 nm range before annealing and is reduced to 50−100 nm after annealing. Meanwhile, PL line widths are reduced by a factor of 2. The improvement in PL properties indicates a restoration of intrinsic PL emissions due to the reparation of the crystal structure. The reduction of the wavelength range for BP of a given thickness (or layer number) will help to relate the layer thickness to emission wavelengths more precisely. This also suggests that the past uncertainty of the relationship between

https://doi.org/10.1021/acsanm.1c00351
ACS Appl. Nano Mater. 2021, 4, 4746−4753

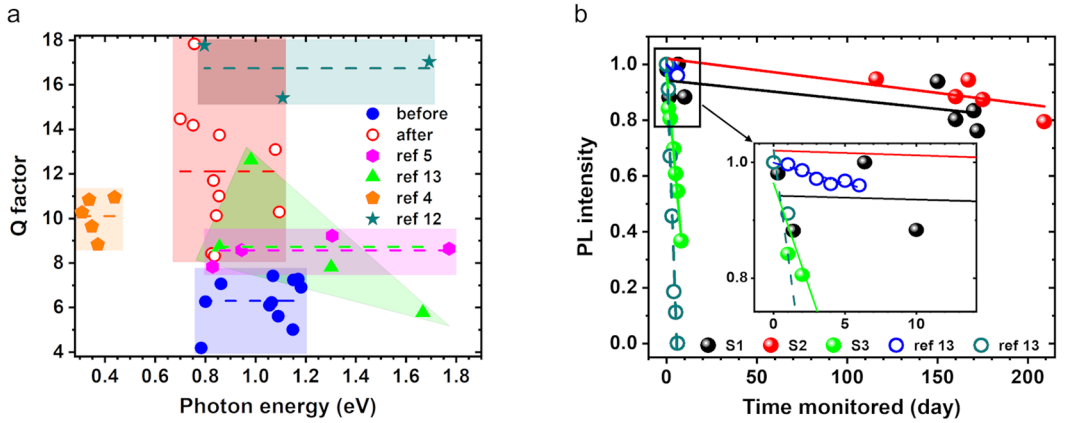

Figure 4. (a) Q factors of PL from various BP samples fabricated by our method before and after annealing. Data extracted from exfoliated (refs 4, 5, 12) and etched (ref 13) BP in literature is present for comparison. The dashed lines in each block are the average Q values for that data group. (b) PL stability comparison. PL intensity evolution with time of our three samples (S1−S3) are presented by solid spheres and linearly fitted by solid lines. Especially sample 3 (S3) is BN/etched BP/BN without annealing. The circles stand for PL evolution of etched BP with (blue circles) and without (dark cyan circles) the ALD Al_2O_3 capping layer,[13] and they are fitted by dashed lines. Our samples show a slower degradation rate.

exciton emission wavelengths and layer numbers originates largely from the poor crystal quality and the related defect emissions of the BP samples. Figure 3c shows the plot of PL peak intensities and wavelengths of 7 BP samples that showed 2L to 3L transition after annealing. In agreement with Figure 3a, PL redshifts correspond to the increase of layer thickness by one monolayer. More importantly, PL intensity is enhanced by a factor between 3 and 200 through annealing, as seen in Figure 3c. The PL enhancement is direct evidence of crystal quality improvement, which is primarily attributed to lattice repair and defect healing[41] through RTA. Other factors such as oxygen incorporation and doping-induced screening effect[42] may also play an important role and are still under investigation. Such PL enhancement makes BP prepared using our method very promising for light-emitting devices especially targeting telecom bands.

Another interesting property of BP is its anisotropy due to the difference in atomic arrangements along with the armchair (AC) and zigzag (ZZ) directions, leading to the anisotropy of optical properties such as absorption and emission. We note that most of the previous reports measured the polarization states of emission and presented the results as the polarization-angle-dependent PL intensity pattern. However, in our case, we measured the total PL emission of all polarizations as the polarization angle of the excitation laser is rotated over 360° by a half-wave plate. Therefore, our measurement reflects absorption anisotropy. In Figure 3d, the excitation-polarization-resolved PL intensity is divided by its maximum (along the AC direction) both before (blue dots) and after (red circles) annealing. We fitted both sets of data by the empirical expression $I(\theta) = A + B\cos^2(\theta)$. We then obtain $I_{AC} = I(0) = A + B$, $I_{ZZ} = I(\pi/2) = A$, where $I_{AC}(I_{ZZ})$ represents the emission intensity when the excitation laser is polarized along with the AC (ZZ) direction. The degree of anisotropy (DOA) is given by $p = \frac{I_{AC} - I_{ZZ}}{I_{AC} + I_{ZZ}}$. The calculated DOA before and after annealing are 0.45 and 0.77, respectively. Due to the dependence of absorption anisotropy on the excitation wavelength[3] as a result of the anisotropic band structure, DOA values obtained by such measurements do not generally agree with DOA obtained from polarized emission measurements. Since our excitation (at λ = 532 nm) is high up in the conduction bands, the anisotropy is weaker than that near the band edge. The polarized emission measurement reflects more of DOA near the band edge. Therefore, our DOA is expected to be smaller than those measured through polarized emission measurement. However, DOA values obtained from the same type of measurements can still reflect the sample quality for different samples. As is shown by theoretical simulations,[43] the existence of defects decreases (increases) the transition strength along the AC (ZZ) direction, reducing the intrinsic anisotropy of BP as a result. Therefore, the improvement of DOA reflected from the polarized absorption measurement demonstrates the restoration of crystallinity of our BP samples through annealing.

Figure 3e shows the comparison of the Raman spectra before and after annealing. We recognize clearly three characteristic Raman modes of BP, A_g^1, B_{2g}, and A_g^2. There is no distinct shift in the Raman peaks after annealing, indicating a negligible change in the basic crystal structure of BP layers. By contrast, peaks of A_g^1 and A_g^2 are significantly increased. Especially for the A_g^2 mode, its peak intensity is multiplied more than two times after annealing. Such increase of Raman signal is consistent with the improved crystal quality after RTA.[18]

It is important to summarize the key evidence of surface reconstruction after RTA. In general, a defective and amorphous layer P_xO_y is formed on top of BP after O_2 plasma etching. Such an amorphous layer cannot be removed or repaired by annealing at a low temperature (e.g., at 225 °C, see Figure 2a,b). However, the amorphous layer disappears after annealing at 450 °C (see Figure 2c,d). In all our annealing experiments at 450 °C, the disappearance of this amorphous layer is accompanied by an increase of BP thickness by one monolayer, as evidenced by PL redshifts (see Figure 3a). Accordingly, the optical quality improves with the significantly enhanced PL peak intensity and the much-reduced line width, as well as enhanced Raman peaks (Figure 3e) after annealing.

To evaluate the optical quality of our samples, we compare the PL features of our samples with those reported in the literature in terms of PL stability and the quality (Q) factor, defined as the center wavelength divided by the line width of a spectrum. The Q factor is a more comparable quantity than absolute line width when measuring the PL quality of materials

https://doi.org/10.1021/acsanm.1c00351
ACS Appl. Nano Mater. 2021, 4, 4746−4753

at different emission wavelengths. Q factors of BP samples prepared by our method before and after annealing are compared with four groups of Q factors extracted from the literature shown in Figure 4a. Without further protection, Q factors of exfoliated FLBP in literature fall in the range of 8−9.[5] In contrast, Q factors of etched FLBP have a larger span from 6 to 13,[13] which may result from the difficulty in controlling sample quality only by etching. With BN protection, Q factors of thicker exfoliated BP (4.5−46 nm) are between 9 and 11.[4] The best Q factors, 15−18, of FLBP are from exfoliated BP sandwiched by BN fabricated in inert gas environment.[12] After annealing, our samples have an average Q factor 12, which is ∼2 times that from before annealing. The average Q values for BN-covered exfoliated, unprotected exfoliated, and etched FLBP are 16.7, 9.4, and 8.7, respectively. Note that protected BP samples here are covered or sandwiched by BN and unprotected BP samples are directly placed on SiO_2/Si substrates. Therefore, our samples have better quality than etched and exfoliated FLBP without protection but not as good as protected FLBP exfoliated in inert gas. Considering the convenience of preparing FLBP in an air environment, FLBP samples made by our method are still competitive.

PL degradation is a severe issue for FLBP. With BN protection and annealing, BP becomes much more stable, making the improved optical properties last for an extended period. The PL evolution measurements of two samples kept in the ambient environment are presented in Figure 4b. We see that PL intensity remains at ∼80% of the original intensity after 170 days and 209 days (∼7 months) for sample 1 (S1) and sample 2 (S2), respectively. To the best of our knowledge, this is so far the most stable PL from FLBP.[37] By contrast, PL of a sample without RTA is also shown, but its PL experienced much more rapid degradation. This indicates that gaps exist between BP and BN. Therefore, the protection is not sufficient by simple BN coverage without gap removal. Note that PL intensity was monitored at the same sample spot for each of the three samples mentioned above. It has been reported that PL intensity of the unprotected exfoliated 2L BP without protection dropped to 1% of the original intensity within 2 min under continuous laser excitation.[15,16] By depositing PECVD SiO_2 as a protection layer, the PL intensity remains at ∼80% after laser excitation for 400 s.[16] Other protection methods such as surface oxygen functional groups[31] and BN coverage[4,12] are used, but no quantitative comparison was made and no long-term PL stability was demonstrated. The most effective protection for FLBP reported[37] seems to be ALD Al_2O_3. PL evolution (in 6 days) of etched BP without further protection (dark cyan circles) and with ALD Al_2O_3 capping layer (blue circles) are presented for comparison.[13] ALD Al_2O_3 protected FLBP shows much slower degradation.[13] PL intensity evolution of our samples and data extracted from the literature are fitted linearly and the slopes reflect the degradation rates. According to the fitted slopes, our annealed samples show the slowest degradation rate and the best stability.

The relationship between PL peak energy and layer thickness is uniquely important for BP and fundamental to the tunability of emission wavelengths through layer numbers. Nevertheless, there has been a large range of uncertainty in this relationship. Figure 5 compares exciton emission energies vs layer number between our measurements and those from existing literature. The gray area stands for the largest PL

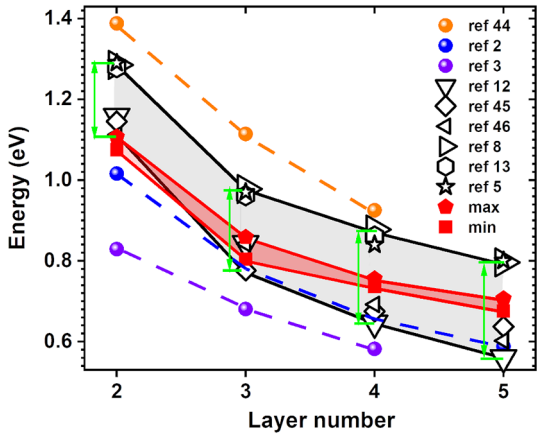

Figure 5. Summary of exciton energies of FLBP. Calculated FLBP bandgaps (ref 44) and exciton energies (refs 2, 3) are presented by spheres in orange, blue, and violet, respectively, and connected by dashed lines. The rest of the data is exciton energies obtained experimentally at room temperature except for ref 12 at 77 K. Exciton energies in refs 12, 45, and 46 are extracted from absorption spectra, and those in refs 8, 5, and 13 are extracted from PL spectra. Red symbols represent our data (max and min) extracted from edges of red rectangle bands in Figure 3b. The areas filled by light gray and red are the energy spans for FLBP reported in the literature so far and our data counterparts.

energy span for 2−5L BP of all results available in the literature.[44−46] The energy overlap between neighboring layer numbers shown by the green lines makes layer determination by PL quite tricky. The red area represents the range of PL peaks from our measurements, given by the edges of the red vertical bands in Figure 3b. In our case, the PL energy spans are determined by the distribution pattern obtained from multiple prepared samples with improved material quality after annealing. The significantly reduced widths of those vertical bands after RTA allow a more accurate relation between PL peak energies and layer number. By comparing the energy spans for 2−5L BP in the literature represented by the green arrows in Figure 5 and the counterparts of our results (red area), the uncertainty ranges of PL peak energy for 2, 3, 4, and 5 layer BP are reduced by 6, 4, 12, and 8 times, respectively, and on average 7 times for 2−5L BP.

CONCLUSIONS

In conclusion, we have demonstrated that O_2 plasma etching combined with BN protection and subsequent thermal annealing provides an effective strategy for preparing high-quality FLBP samples. The significantly improved or largely restored intrinsic optical properties are evidenced by many excellent photoluminescence features, including PL enhancement by up to 200 times, line width reduction by a factor of 2, restoration of intrinsic anisotropy of BP, and vastly increased stability. Importantly, our prepared samples maintained 80% of the initial optical emission intensity after almost 7 months (209 days) in the typical ambient environment. Our study reveals an interesting lattice reconstruction and restoration from defective and amorphous P_xO_y to crystalline-like BP through high-temperature annealing. The PL comparison before and after annealing provides a more definite relation between PL peak energy and layer number, an important relationship for BP. We believe that our sample preparation strategy can enable more consistent production of high-quality

https://doi.org/10.1021/acsanm.1c00351
ACS Appl. Nano Mater. 2021, 4, 4746−4753

FLBP samples in the future for both basic science studies and device exploration. The optical properties revealed by our systematic study could add more clarity and consistency to the rapidly expanding literature of BP research. The high-quality, long-lasting BP samples with more intrinsic optical properties establish BP as an important photonic material with wavelength tunability in a wide range of near-infrared wavelengths through layer number control. Such a unique tuning capability of emission and absorption properties among 2D layered materials could enable 2D-based nanolasers that work in an unprecedented extensive wavelength range from the near- to mid-infrared with the same material by simply adjusting the layer number. Similarly, multiband detectors and modulators can be fabricated using FLBP. The lack of silicon absorption for BP thicker than three monolayers could make such silicon-based devices even more appealing.

METHODS

Sample Preparation. Scotch tape and Nitto SPV224 blue tape were used to exfoliate BP flakes from bulk material (Smart Elements) and further thin down the flakes. The key to obtaining uniform thin (~10 nm) BP flake is to minimize ripping times so that flakes are large and with flat interfaces. Exfoliation of BN (hq graphene) follows the same rule. Then the tape with 2D material flakes is placed onto PDMS and pressed gently to squeeze bubbles out. By peeling off the tape fast, flakes can be left on the PDMS. Transfer onto a SiO_2/Si substrate is completed by tightly contacting PDMS with the substrate and then slowly lifting the PDMS on a ceramic heater at 35 °C. For an ~10 nm thick BP, the general etching conditions for the first run are 30 W bias power and 400 W RF power under 50 mTorr pressure with 30 sccm O_2 flow for 4 min (Plasma-Therm Apex ICP). The second run is generally under 30 mTorr, with other conditions unchanged for ~1 to ~2 min (see Supporting Information S3).

Scanning Transmission Electron Microscopy (STEM). The BN/etched-BP/BN and BN/exfoliated-BP/BN slice specimens for STEM imaging were prepared by using a FEI Nova 200 Dual-Beam focused ion beam (FIB) system with a Ga ion source. Cross-sectional STEM images were obtained by using a JEOL-ARM200F microscope operated at 200 kV.

Photoluminescence (PL). PL measurements were done at room temperature using a home-built system, where a 532 nm diode laser under continuous-wave operation was used as the excitation source. The incident laser was focused to a spot with a diameter of ~3 μm by using a 50× NIR Mitutoyo objective. The PL spectrum was collected by using an extended InGaAs array detector (Symphony II) coupled to Horiba monochromator (iHR 320).

ASSOCIATED CONTENT

Supporting Information

The Supporting Information is available free of charge at https://pubs.acs.org/doi/10.1021/acsanm.1c00351.

> More information on effects of annealing temperature; PL of exfoliated few-layer BP; O_2 plasma etching conditions; PL spectra comparison before and after annealing; and sample homogeneity (PDF)

AUTHOR INFORMATION

Corresponding Author

Cun-Zheng Ning − *School of Electrical, Computer and Energy Engineering, Arizona State University, Tempe, Arizona 85287, United States*; Email: cning@asu.edu

Authors

Dongying Li − *School of Electrical, Computer and Energy Engineering, Arizona State University, Tempe, Arizona 85287, United States*; orcid.org/0000-0003-3434-9924

Yueyang Yu − *School of Electrical, Computer and Energy Engineering, Arizona State University, Tempe, Arizona 85287, United States*

Complete contact information is available at: https://pubs.acs.org/10.1021/acsanm.1c00351

Notes

The authors declare no competing financial interest.

ACKNOWLEDGMENTS

The authors thank Kenneth Mossman and Manuel A. Roldan Gutierrez for STEM characterization. We gratefully acknowledge the use of facilities at the NanoFab and Eyring Materials Center at Arizona State University. This work was supported by the NSF under Grant ECCS-1807644.

REFERENCES

(1) Xia, F.; Wang, H.; Jia, Y. Rediscovering Black Phosphorus as an Anisotropic Layered Material for Optoelectronics and Electronics. *Nat. Commun.* **2014**, *5*, 4458.

(2) Qiao, J.; Kong, X.; Hu, Z.-X.; Yang, F.; Ji, W. High-Mobility Transport Anisotropy and Linear Dichroism in Few-Layer Black Phosphorus. *Nat. Commun.* **2014**, *5*, 4475.

(3) Tran, V.; Soklaski, R.; Liang, Y.; Yang, L. Layer-Controlled Band Gap and Anisotropic Excitons in Few-Layer Black Phosphorus. *Phys. Rev. B: Condens. Matter Mater. Phys.* **2014**, *89* (23), 235319.

(4) Chen, C.; Chen, F.; Chen, X.; Deng, B.; Eng, B.; Jung, D.; Guo, Q.; Yuan, S.; Watanabe, K.; Taniguchi, T.; Lee, M. L.; Xia, F. Bright Mid-Infrared Photoluminescence from Thin-Film Black Phosphorus. *Nano Lett.* **2019**, *19*, 1488.

(5) Yang, J.; Xu, R.; Pei, J.; Myint, Y. W.; Wang, F.; Wang, Z.; Zhang, S.; Yu, Z.; Lu, Y. Optical Tuning of Exciton and Trion Emissions in Monolayer Phosphorene. *Light: Sci. Appl.* **2015**, *4* (7), No. e312.

(6) Chang, T.-Y.; Chen, Y.; Luo, D.-I.; Li, J.-X.; Chen, P.-L.; Lee, S.; Fang, Z.; Li, W.-Q.; Zhang, Y.-Y.; Li, M.; Majumdar, A.; Liu, C.-H. Black Phosphorus Mid-Infrared Light-Emitting Diodes Integrated with Silicon Photonic Waveguides. *Nano Lett.* **2020**, *20* (9), 6824−6830.

(7) Zong, X.; Hu, H.; Ouyang, G.; Wang, J.; Shi, R.; Zhang, L.; Zeng, Q.; Zhu, C.; Chen, S.; Cheng, C.; Wang, B.; Zhang, H.; Liu, Z.; Huang, W.; Wang, T.; Wang, L.; Chen, X. Black Phosphorus-Based van Der Waals Heterostructures for Mid-Infrared Light-Emission Applications. *Light: Sci. Appl.* **2020**, *9* (1), 114.

(8) Zhang, S.; Yang, J.; Xu, R.; Wang, F.; Li, W.; Ghufran, M.; Zhang, Y.-W.; Yu, Z.; Zhang, G.; Qin, Q.; Lu, Y. Extraordinary Photoluminescence and Strong Temperature/Angle-Dependent Raman Responses in Few-Layer Phosphorene. *ACS Nano* **2014**, *8* (9), 9590−9596.

(9) Li, Y.; Zhang, J.; Huang, D.; Sun, H.; Fan, F.; Feng, J.; Wang, Z.; Ning, C. Z. Room-Temperature Continuous-Wave Lasing from Monolayer Molybdenum Ditelluride Integrated with a Silicon Nanobeam Cavity. *Nat. Nanotechnol.* **2017**, *12* (10), 987−992.

(10) Bie, Y.-Q.; Grosso, G.; Heuck, M.; Furchi, M. M.; Cao, Y.; Zheng, J.; Bunandar, D.; Navarro-Moratalla, E.; Zhou, L.; Efetov, D. K.; Taniguchi, T.; Watanabe, K.; Kong, J.; Englund, D.; Jarillo-Herrero, P. A MoTe 2 -Based Light-Emitting Diode and Photodetector for Silicon Photonic Integrated Circuits. *Nat. Nanotechnol.* **2017**, *12* (12), 1124−1129.

(11) Zhou, Q.; Chen, Q.; Tong, Y.; Wang, J. Light-Induced Ambient Degradation of Few-Layer Black Phosphorus: Mechanism and Protection. *Angew. Chem., Int. Ed.* **2016**, *55* (38), 11437−11441.

(12) Li, L.; Kim, J.; Jin, C.; Ye, G. J.; Qiu, D. Y.; da Jornada, F. H.; Shi, Z.; Chen, L.; Zhang, Z.; Yang, F.; Watanabe, K.; Taniguchi, T.; Ren, W.; Louie, S. G.; Chen, X. H.; Zhang, Y.; Wang, F. Direct Observation of the Layer-Dependent Electronic Structure in Phosphorene. *Nat. Nanotechnol.* **2017**, *12* (1), 21−25.
(13) Pei, J.; Gai, X.; Yang, J.; Wang, X.; Yu, Z.; Choi, D.-Y.; Luther-Davies, B.; Lu, Y. Producing Air-Stable Monolayers of Phosphorene and Their Defect Engineering. *Nat. Commun.* **2016**, *7*, 10450.
(14) Zhang, G.; Huang, S.; Wang, F.; Xing, Q.; Song, C.; Wang, C.; Lei, Y.; Huang, M.; Yan, H. The Optical Conductivity of Few-Layer Black Phosphorus by Infrared Spectroscopy. *Nat. Commun.* **2020**, *11* (1), 1847.
(15) Khatibi, A.; Godiksen, R. H.; Basuvalingam, S. B.; Pellegrino, D.; Bol, A. A.; Shokri, B.; Curto, A. G. Anisotropic Infrared Light Emission from Quasi-1D Layered TiS 3. *2D Mater.* **2020**, *7* (1), 015022.
(16) Khatibi, A.; Petruzzella, M.; Shokri, B.; Curto, A. G. Defect Engineering in Few-Layer Black Phosphorus for Tunable and Photostable Infrared Emission. *Opt. Mater. Express* **2020**, *10* (7), 1488.
(17) Wang, F.; Zhang, G.; Huang, S.; Song, C.; Wang, C.; Xing, Q.; Lei, Y.; Yan, H. Electronic Structures of Air-Exposed Few-Layer Black Phosphorus by Optical Spectroscopy. *Phys. Rev. B: Condens. Matter Mater. Phys.* **2019**, *99* (7), 075427.
(18) Favron, A.; Gaufrès, E.; Fossard, F.; Phaneuf-L'Heureux, A.-L.; Tang, N. Y.-W.; Lévesque, P. L.; Loiseau, A.; Leonelli, R.; Francoeur, S.; Martel, R. Photooxidation and Quantum Confinement Effects in Exfoliated Black Phosphorus. *Nat. Mater.* **2015**, *14* (8), 826−832.
(19) Walia, S.; Sabri, Y.; Ahmed, T.; Field, M. R.; Ramanathan, R.; Arash, A.; Bhargava, S. K.; Sriram, S.; Bhaskaran, M.; Bansal, V.; Balendhran, S. Defining the Role of Humidity in the Ambient Degradation of Few-Layer Black Phosphorus. *2D Mater.* **2017**, *4* (1), 015025.
(20) Niu, X.; Li, Y.; Zhang, Y.; Li, Q.; Zhou, Q.; Zhao, J.; Wang, J. Photo-Oxidative Degradation and Protection Mechanism of Black Phosphorus: Insights from Ultrafast Dynamics. *J. Phys. Chem. Lett.* **2018**, *9* (17), 5034−5039.
(21) Yasaei, P.; Kumar, B.; Foroozan, T.; Wang, C.; Asadi, M.; Tuschel, D.; Indacochea, J. E.; Klie, R. F.; Salehi-Khojin, A. High-Quality Black Phosphorus Atomic Layers by Liquid-Phase Exfoliation. *Adv. Mater.* **2015**, *27* (11), 1887−1892.
(22) Hanlon, D.; Backes, C.; Doherty, E.; Cucinotta, C. S.; Berner, N. C.; Boland, C.; Lee, K.; Harvey, A.; Lynch, P.; Gholamvand, Z.; Zhang, S.; Wang, K.; Moynihan, G.; Pokle, A.; Ramasse, Q. M.; McEvoy, N.; Blau, W. J.; Wang, J.; Abellan, G.; Hauke, F.; Hirsch, A.; Sanvito, S.; O'Regan, D. D.; Duesberg, G. S.; Nicolosi, V.; Coleman, J. N. Liquid Exfoliation of Solvent-Stabilized Few-Layer Black Phosphorus for Applications beyond Electronics. *Nat. Commun.* **2015**, *6* (1), 8563.
(23) Brent, J. R.; Savjani, N.; Lewis, E. A.; Haigh, S. J.; Lewis, D. J.; O'Brien, P. Production of Few-Layer Phosphorene by Liquid Exfoliation of Black Phosphorus. *Chem. Commun.* **2014**, *50* (87), 13338−13341.
(24) Jeong, M.-H.; Kwak, D.-H.; Ra, H.-S.; Lee, A.-Y.; Lee, J.-S. Realizing Long-Term Stability and Thickness Control of Black Phosphorus by Ambient Thermal Treatment. *ACS Appl. Mater. Interfaces* **2018**, *10* (22), 19069−19075.
(25) Yang, S.; Kim, A.; Park, J.; Kwon, H.; Lanh, P. T.; Hong, S.; Kim, K. J.; Kim, J. W. Thermal Annealing of Black Phosphorus for Etching and Protection. *Appl. Surf. Sci.* **2018**, *457*, 773−779.
(26) Kwon, H.; Seo, S. W.; Kim, T. G.; Lee, E. S.; Lanh, P. T.; Yang, S.; Ryu, S.; Kim, J. W. Ultrathin and Flat Layer Black Phosphorus Fabricated by Reactive Oxygen and Water Rinse. *ACS Nano* **2016**, *10* (9), 8723−8731.
(27) Jia, J.; Jang, S. K.; Lai, S.; Xu, J.; Choi, Y. J.; Park, J.-H.; Lee, S. Plasma-Treated Thickness-Controlled Two-Dimensional Black Phosphorus and Its Electronic Transport Properties. *ACS Nano* **2015**, *9* (9), 8729−8736.
(28) Lee, G.; Lee, J.-Y.; Lee, G.-H.; Kim, J. Tuning the Thickness of Black Phosphorus via Ion Bombardment-Free Plasma Etching for Device Performance Improvement. *J. Mater. Chem. C* **2016**, *4* (26), 6234−6239.
(29) Alsaffar, F.; Alodan, S.; Alrasheed, A.; Alhussain, A.; Alrubaiq, N.; Abbas, A.; Amer, M. R. Raman Sensitive Degradation and Etching Dynamics of Exfoliated Black Phosphorus. *Sci. Rep.* **2017**, *7*, 44540.
(30) Zhao, Y.; Zhou, Q.; Li, Q.; Yao, X.; Wang, J. Passivation of Black Phosphorus via Self-Assembled Organic Monolayers by van Der Waals Epitaxy. *Adv. Mater.* **2017**, *29* (6), 1603990.
(31) Ryder, C. R.; Wood, J. D.; Wells, S. A.; Yang, Y.; Jariwala, D.; Marks, T. J.; Schatz, G. C.; Hersam, M. C. Covalent Functionalization and Passivation of Exfoliated Black Phosphorus via Aryl Diazonium Chemistry. *Nat. Chem.* **2016**, *8* (6), 597−602.
(32) Zhao, Y.; Wang, H.; Huang, H.; Xiao, Q.; Xu, Y.; Guo, Z.; Xie, H.; Shao, J.; Sun, Z.; Han, W.; Yu, X.-F.; Li, P.; Chu, P. K. Surface Coordination of Black Phosphorus for Robust Air and Water Stability. *Angew. Chem., Int. Ed.* **2016**, *55* (16), 5003−5007.
(33) Wood, J. D.; Wells, S. A.; Jariwala, D.; Chen, K.-S.; Cho, E.; Sangwan, V. K.; Liu, X.; Lauhon, L. J.; Marks, T. J.; Hersam, M. C. Effective Passivation of Exfoliated Black Phosphorus Transistors against Ambient Degradation. *Nano Lett.* **2014**, *14* (12), 6964−6970.
(34) Illarionov, Y. Y.; Waltl, M.; Rzepa, G.; Knobloch, T.; Kim, J.-S.; Akinwande, D.; Grasser, T. Highly-Stable Black Phosphorus Field-Effect Transistors with Low Density of Oxide Traps. *Npj 2D Mater. Appl.* **2017**, *1* (1), 1−7.
(35) Avsar, A.; Vera-Marun, I. J.; Tan, J. Y.; Watanabe, K.; Taniguchi, T.; Castro Neto, A. H.; Özyilmaz, B. Air-Stable Transport in Graphene-Contacted, Fully Encapsulated Ultrathin Black Phosphorus-Based Field-Effect Transistors. *ACS Nano* **2015**, *9* (4), 4138−4145.
(36) Chen, X.; Wu, Y.; Wu, Z.; Han, Y.; Xu, S.; Wang, L.; Ye, W.; Han, T.; He, Y.; Cai, Y.; Wang, N. High-Quality Sandwiched Black Phosphorus Heterostructure and Its Quantum Oscillations. *Nat. Commun.* **2015**, *6* (1), 7315.
(37) Abate, Y.; Akinwande, D.; Gamage, S.; Wang, H.; Snure, M.; Poudel, N.; Cronin, S. B. Recent Progress on Stability and Passivation of Black Phosphorus. *Adv. Mater.* **2018**, *30* (29), 1704749.
(38) Fortin-Deschênes, M.; Levesque, P. L.; Martel, R.; Moutanabbir, O. Dynamics and Mechanisms of Exfoliated Black Phosphorus Sublimation. *J. Phys. Chem. Lett.* **2016**, *7* (9), 1667−1674.
(39) Liu, X.; Wood, J. D.; Chen, K.-S.; Cho, E.; Hersam, M. C. In Situ Thermal Decomposition of Exfoliated Two-Dimensional Black Phosphorus. *J. Phys. Chem. Lett.* **2015**, *6* (5), 773−778.
(40) Tian, H.; Guo, Q.; Xie, Y.; Zhao, H.; Li, C.; Cha, J. J.; Xia, F.; Wang, H. Anisotropic Black Phosphorus Synaptic Device for Neuromorphic Applications. *Adv. Mater.* **2016**, *28* (25), 4991−4997.
(41) Surrente, A.; Dumcenco, D.; Yang, Z.; Kuc, A.; Jing, Y.; Heine, T.; Kung, Y.-C.; Maude, D. K.; Kis, A.; Plochocka, P. Defect Healing and Charge Transfer-Mediated Valley Polarization in MoS2/MoSe2/MoS2 Trilayer van Der Waals Heterostructures. *Nano Lett.* **2017**, *17* (7), 4130−4136.
(42) Kinoshita, A.; Hirayama, H.; Riblet, P.; Ainoya, M.; Hirata, A.; Aoyagi, Y. Emission Enhancement of GaN/AlGaN Single-Quantum-Wells Due to Screening of Piezoelectric Field. *MRS Internet J. Nitride Semicond. Res.* **2000**, *5* (S1), 682−688.
(43) Yuan, S.; Rudenko, A. N.; Katsnelson, M. I. Transport and Optical Properties of Single- and Bilayer Black Phosphorus with Defects. *Phys. Rev. B: Condens. Matter Mater. Phys.* **2015**, *91* (11), 115436.
(44) Tran, V.; Fei, R.; Yang, L. Quasiparticle Energies, Excitons, and Optical Spectra of Few-Layer Black Phosphorus. *2D Mater.* **2015**, *2* (4), 044014.
(45) Zhang, G.; Huang, S.; Chaves, A.; Song, C.; Özçelik, V. O.; Low, T.; Yan, H. Infrared Fingerprints of Few-Layer Black Phosphorus. *Nat. Commun.* **2017**, *8*, 14071.
(46) Zhang, G.; Chaves, A.; Huang, S.; Wang, F.; Xing, Q.; Low, T.; Yan, H. Determination of Layer-Dependent Exciton Binding Energies in Few-Layer Black Phosphorus. *Sci. Adv.* **2018**, *4* (3), No. eaap9977.

https://doi.org/10.1021/acsanm.1c00351
ACS Appl. Nano Mater. 2021, 4, 4746−4753